# Adaptive Tracking Control of Nonlinear Multi-Agent Systems Subject to Multiple Constraints via Multi-Dimensional Taylor Network

Wei-Jie Hao, Zhao-Yi Zong, Shu-Zhen Wei, Shan-Liang Zhu, and Yu-Qun Han

***Abstract*—This paper investigates the adaptive tracking control problem for nonlinear multi-agent systems operating under simultaneous input saturation and output performance constraints. To address asymmetric input saturation, an innovative auxiliary system is developed that generates compensatory signals based on the discrepancy between the input signal and the saturation function output. A central contribution is the introduction of a novel dynamic performance function (DPF), this function leverages signals from the auxiliary system to adaptively adjust performance boundaries, critically activating this adjustment only when input saturation occurs concurrently with synchronization errors exceeding predefined safety limits, thereby effectively resolving conflicts between the input and performance constraints. Furthermore, a first-order filter is employed within the backstepping control design to approximate virtual control derivatives, mitigating the "computational explosion" issue. An adaptive controller incorporating multi-dimensional Taylor network (MTN) is then synthesized based on this framework. Rigorous Lyapunov stability analysis confirms the boundedness of all signals within the closed-loop system. Supporting this theoretical finding, simulation results confirm the proposed control strategy's effectiveness and feasibility, demonstrating enhanced synchronization performance and robustness under these multiple, potentially conflicting constraints.**

***Note to Practitioners*—Practitioners working with nonlinear multi-agent systems facing input and output constraints should consider the adaptive tracking control approach presented in this paper. The method innovatively addresses asymmetric input saturation by developing an auxiliary system that generates compensatory signals to mitigate its negative effects on system performance. To balance input saturation and output performance constraints, a dynamic performance function is introduced, ensuring that synchronization errors stay within acceptable ranges. This approach is particularly valuable for applications like drone swarms or automated transportation systems, where synchronization and constraint adherence are safety-critical.**

***Index Terms*—Multi-agent systems, input constraints, output constraints, multi-dimensional Taylor network.**

Received 10 February 2025; revised 29 April 2025; accepted 15 June 2025. Date of publication 19 June 2025; date of current version 26 June 2025. This article was recommended for publication by Associate Editor D. Famularo and Editor S. Takai upon evaluation of the reviewers' comments. This work was supported by Shandong Provincial Natural Science Foundation, China under Grant ZR2020QF055. *(Corresponding author: Yu-Qun Han.)*

The authors are with the School of Mathematics and Physics, Qingdao University of Science and Technology, Qingdao 266061, China (e-mail: yuqunhan@163.com).

Digital Object Identifier 10.1109/TASE.2025.3581459

## I. Introduction

MULTI-AGENT systems consist of multiple agents and have attracted considerable attention owing to their diverse applications across various interdisciplinary fields, such as artificial intelligence [1], aerospace systems [2], and power systems [3]. Among the primary issues in multi-agent systems research, the consensus problem is of particular importance [4], [5]. Consensus in multi-agent systems refers to the process by which each agent, through local cooperation and communication, continuously adjusts its behavior until all agents achieve the same state, a critical requirement for coordinated control. In recent years, nonlinear multi-agent systems have received extensive attention [6], [7]. In particular, methods such as fuzzy control [8], [9], [10] and radial basis function (RBF) neural networks [11], [12] have been employed to handle system nonlinearities, demonstrating promising results when combined with traditional adaptive control. Among these methods, the multi-dimensional Taylor network (MTN) [13], [14], [15], [16], a distinctive neural network architecture, has been recognized as an efficient and effective approach for addressing system nonlinearities due to its simplicity and powerful approximation capabilities. However, despite its potential, MTN has yet to be widely applied in controlling nonlinear multi-agent systems that face both input and output constraints, thereby limiting its broader development and application in complex multi-agent system control scenarios. Therefore, exploring effective methods to control nonlinear multi-agent systems with multiple constraints remains a critical and promising research avenue.

In practical systems, due to the inherent physical constraints of actuators, nonlinear systems often encounter input saturation limitations. Such constraints can adversely affect system performance and may even lead to instability. Considering the significant influence of input saturation on system performance and stability, comprehensive research on this phenomenon is crucial. Two primary approaches currently exist for addressing input saturation: the approximation approach, which transforms the saturation model into a linear model with errors [17], [18], [19], [20], and the auxiliary system approach, which generates auxiliary signals to mitigate the effects of input saturation [21], [22], [23]. Recently, nonlinear systems with input saturation constraints have emerged as a focal point of research, attracting considerable attention and leading to notable advancements. These include studies

on uncertain nonlinear multi-agent systems [24], [25], event-triggered nonlinear multi-agent systems [26], and time-delay nonlinear multi-agent systems [27]. Despite the significant progress made in understanding the effects of input saturation on nonlinear multi-agent systems, these studies have primarily focused on input constraints while offering limited exploration of output constraints.

Output constraints in nonlinear multi-agent systems refer to a specific type of state constraint that requires each agent's output to remain strictly within predefined limits. This ensures that the system meets specified performance criteria, thereby ensuring overall system performance and stability. Therefore, addressing output constraints is crucial when designing and controlling nonlinear multi-agent systems. Recently, funnel control (FC) [28], [29] and prescribed performance control (PPC) [30], [31], [32], [33], [34] have been proposed as solutions for addressing output constraints. PPC achieves performance guarantees by transforming the original system into an equivalent "unconstrained" system via performance functions and coordinate transformations, combined with barrier Lyapunov functions. Many results have been obtained for nonlinear multi-agent systems with output constraints, as shown in [35], [36], [37], and [38]. However, in cases of input saturation, system performance can degrade due to insufficient actuator input. Flexible performance control (FPC) has been introduced to address this issue. In [39], the FPC method was employed, with an auxiliary system designed to ensure that all states remain non-negative, allowing the system to self-adjust in the presence of input saturation. In [40], a new flexible fixed-time performance function was designed to guarantee performance constraints in switched nonlinear systems with input saturation. While preliminary advancements have been made in controlling nonlinear multi-agent systems with multiple constraints, research in this area remains limited.

Motivated by the preceding observations, this work develops a novel adaptive control method utilizing MTN for nonlinear multi-agent systems operating under concurrent input and output constraints. The principal contributions of this research are detailed as follows:

1) A central innovation of this work is the development of a dynamic performance function (DPF) specifically engineered to resolve the inherent conflict between input saturation and output performance constraints. Distinct from prior approaches [39] and [40], DPF implements a conditional adaptation strategy: the performance boundaries are dynamically adjusted if and only if input saturation occurs concurrently and the synchronization error exceeds a predefined safety threshold. This targeted mechanism addresses the constraint conflict with precision, avoiding unnecessary relaxation of performance bounds and ensuring stability adaptation occurs only when genuinely necessitated by the combined effect of saturation and error magnitude.
2) A novel auxiliary system, tailored for asymmetric input saturation, is proposed and synergistically integrated with the DPF. The non-negative signals generated by this auxiliary system, directly reflecting the saturation status and error condition relative to safety limits, serve as the key enabling trigger for the DPF's boundary adaptation logic. This approach circumvents the complexity and potential inaccuracies associated with the smooth function approximations often employed in traditional saturation handling methods [20]. Furthermore, these non-negative signals are utilized within the DPF structure to dynamically define the performance boundaries, ensuring synchronization errors are constrained within specified ranges, thereby simultaneously satisfying the output constraints.
3) A computationally feasible framework is developed for nonlinear multi-agent systems with simultaneous input and output constraints by integrating MTN-based adaptation with command-filtered backstepping. The crucial use of a first-order filter mitigates "computational explosion", thereby enhancing the practical scalability and applicability of the proposed adaptive control strategy for higher-order systems under these coupled constraints.

## II. Preliminaries and Formulation

### A. Theory of Graph

The communication topology within a multi-agent system can be modeled by a directed graph $\mathcal{K} = (\mathcal{P}, \mathcal{G}, \mathcal{M})$. Here, $\mathcal{P} = \{1, 2, \ldots, N\}$ constitutes the set of nodes, $\mathcal{G}$ is the set of edges, and the adjacency matrix $\mathcal{M} = [m_{i,j}] \in \mathfrak{R}^{N\times N}$ characterizes the information flow pathways. An element $m_{i,j} > 0$ signifies that agent $i$ receives information from agent $j$, whereas $m_{i,j} = 0$ indicates the absence of this directed link. Accordingly, vertex $j$ is designated as a neighbor of vertex $i$ if $m_{i,j} > 0$. The in-degree of vertex $i$ is computed as $m_i = \sum_{j=1}^{N} m_{i,j}$. Finally, the graph Laplacian matrix is formulated as $\mathcal{L}=\mathcal{D}-\mathcal{M}$, where $\mathcal{D} = diag(m_1, \ldots, m_N)$ represents the diagonal matrix of in-degrees.

### B. System Description

Consider a class of multi-agent systems with input saturation

$$\begin{cases} \dot{x}_{i,j} = x_{i,j+1} + w_{i,j}\left(\bar{x}_{i,j}\right) + \Delta_{i,j}(t) \\ \dot{x}_{i,n} = p_i(u_i) + w_{i,n}\left(\bar{x}_{i,n}\right) + \Delta_{i,n}(t) \\ y_i = x_{i,1}, i = 1, \ldots, N, j = 1, \ldots, n-1 \end{cases} \tag{1}$$

where $\boldsymbol{x}_{i,j}^{-} = \left[x_{i,1}, x_{i,2}, \cdots, x_{i,j}\right]^{\mathrm{T}} \in \mathfrak{R}^{j}$ represents the state vector for the $i-$th follower agent. The corresponding control input and system output are denoted by $u_i \in \mathfrak{R}$ and $y_i \in \mathfrak{R}$, respectively. The dynamics incorporate an unmodeled smooth function $w_{i,j}\left(\bar{x}_{i,j}\right)$ fulfilling the property $w_{i,j}(\mathbf{0}) = 0$, and $\Delta_{i,j}(t)$ represents unknown external disturbances, satisfying $\left|\Delta_{i,j}(t)\right| < \bar{\Delta}_{i,j}$, where $\bar{\Delta}_{i,j} > 0$ denotes unknown constants. $p_i(u_i)$ represents the asymmetric input saturation function as follows

$$p_i(u_i) = \begin{cases} \underline{\vartheta}_i, & u_i < \underline{\vartheta}_i \\ u_i, & \underline{\vartheta}_i \le u_i \le \bar{\vartheta}_i \\ \bar{\vartheta}_i, & u_i > \bar{\vartheta}_i \end{cases} \tag{2}$$

where $\bar{\vartheta}_i = p_{i,\max} > 0$, $\underline{\vartheta}_i = p_{i,\min} < 0$ represent the upper and lower bound, respectively.

To address input saturation in the system, an auxiliary system is constructed to mitigate this issue

$$\begin{cases} \dot{\phi}_{i,1} = -k_{i,1}\phi_{i,1} + m_{i,1}B_i\phi_{i,2} \\ \dot{\phi}_{i,j} = -k_{i,j}\phi_{i,j} + \phi_{i,j+1}, j = 2,\ldots,n \end{cases} \tag{3}$$

where $\phi_{i,j}$ represents the state of the auxiliary system and $\phi_{i,j}(0) = 0$. $\phi_{i,j+1} = \Delta u_i = p_i(u_i) - u_i$. $k_{i,j} > 0$ is a constant. $B_i$ and $m_{i,1}$ will be defined later.

*Assumption 1 [41]:* It is assumed that the communication graph contains a spanning tree rooted at the leader node.

Considering the signal of the leader

$$\dot{y}_f = g(y_f, t) \tag{4}$$

wherein $y_f$ signifies the leader's output trajectory, while $g(y_f, t)$ is a specified function.

For follower $i$, the corresponding synchronization error is formulated by

$$e_i = \sum_{j=1}^{N} m_{i,j}(y_i - y_j) + b_i(y_i - y_f) \tag{5}$$

where $b_i \geq 0$ denote the edge weight connecting the leader to follower $i$. When follower $i$ is unable to access information from the leader, $b_i = 0$. Let $B_i = M_i + b_i$, and $M_i = \sum_{j=1}^{N} m_{i,j}$.

*Assumption 2 [42]:* Continuity and boundedness are assumed for the leader signal $y_f$, and its derivatives with respect to time up to order $n$.

*Control Objective:* Designing an adaptive tracking controller based on MTN to guarantee the following:

(1) Guarantee the boundedness of all signals within the closed-loop system.
(2) The synchronization error $e_i$ always constrained within a specified boundary $-\zeta_{i,2}^* < e_i < \zeta_{i,1}^*$.

### C. Dynamic Performance Function

Firstly, the time-varying function $\eta_i(t)$ is defined as follows

$$\eta_i(t) = \left(\eta_{i,0} - \eta_{i,\infty}\right) g_i(t) + \eta_{i,\infty} \tag{6}$$

where $\eta_{i,0}$ and $\eta_{i,\infty}$ are the positive constants satisfying $0 < \eta_{i,\infty} < \eta_{i,0} \leq 1$. The time-varying function $g_i(x)$ is a smoothly monotonic function, and its $(n+1) - th$ derivative is continuously bounded, satisfying the conditions $g_i(0) = 1$ and $\lim_{t\to\infty} g_i(t) = 0$. Thus, it can be deduced that $\eta_{i,0} = \eta_i(0)$, $\lim_{t\to\infty} \eta_i(t) = \eta_{i,\infty} = \eta_i(\infty)$, and $\eta_i(t)$ is monotonically decreasing.

An auxiliary barrier function can be formulated as follows

$$\zeta\left(\rho_{i,m}(t)\right) = \frac{v_i}{2} \ln \frac{1 + \rho_{i,m}}{1 - \rho_{i,m}} \tag{7}$$

where $v_i > 0$ is a constant. The function $\rho_{i,m}(t)$ satisfies $\rho_{i,m} = \eta_i(t)\mu_{i,m}$, and $\mu_{i,m}$ is a constant satisfying the condition $\mu_{i,m} \in (0, 1]$, where $i = 1,\ldots,N$ and $m = 1, 2$.

To simultaneously resolve the predefined performance objectives and input saturation challenges, a novel auxiliary system is developed by extending a traditional auxiliary system, which is specifically tailored to effectively handle input saturation. This auxiliary system is employed in the formulation of the performance function.

Define the auxiliary system as

$$\iota_{i,m,j} = -b_{i,m,j}\iota_{i,m,j} + d_{i,m,j}\iota_{i,m,j+1} \tag{8}$$

where $\iota_{i,m,j}$ represents the state of the auxiliary system and $\iota_{i,m,j}(0) = 0$. $b_{i,k,j} > 0$ and $d_{i,k,j} > 0$ are constants. $\iota_{i,1,n+1}$ and $\iota_{i,2,n+1}$ satisfy the following conditions

$$\begin{cases} \iota_{i,1,n+1} = \left[\xi^*\left(e_i - \chi_i\zeta\left(\rho_{i,1}(t)\right)\right) + 1\right]|\Delta u_i| \\ \iota_{i,2,n+1} = \left[\xi^*\left(-e_i - \chi_i\zeta\left(\rho_{i,2}(t)\right)\right) + 1\right]|\Delta u_i| \end{cases} \tag{9}$$

where the parameter $\chi_i$ satisfies $0 < \chi_i < 1$. The piecewise function $\xi^*(x)$ satisfies the following conditions $\begin{cases} \xi^*(x) = 1, x \geq 0 \\ \xi^*(x) = -1, x < 0 \end{cases}$.

Additionally, the following positive function $\gamma_{i,m}(t)$ is defined as

$$\gamma_{i,m}(t) = \left(1 - \frac{1}{\eta_i(t)\mu_{i,m}}\right) e^{-\eta_{i,m}^*} + \frac{1}{\eta_i(t)\mu_{i,m}} \tag{10}$$

where $\eta_{i,m}^* = R_{i,m}\arctan\left(\iota_{i,m,1}\right)$, and $R_{i,m} > 0$ is a constant.

Next, the dynamic performance function is formulated as follows

$$\zeta_{i,m}^* = \frac{v_i}{2} \ln \frac{1 + \tilde{\rho}_{i,m}}{1 - \tilde{\rho}_{i,m}} \tag{11}$$

where $\tilde{\rho}_{i,m} = \eta_i(t)\mu_{i,m}\gamma_{i,m}(t) \leq 1$. From the definition of $\zeta_{i,m}^*$, it can be observed that the function is monotonically increasing with respect to the function $\tilde{\rho}_{i,m}$.

*Remark 1:* The monotonic decrease of the time-varying function $\eta_i(t)$ from its initial value $\eta_{i,0} = \eta_i(0)$ to its final value $\lim_{t\to\infty} \eta_i(t) = \eta_{i,\infty} = \eta_i(\infty)$ is a key feature ensuring a smooth and predictable evolution of the performance boundaries defined later via $\rho_{i,m}(t)$. To guarantee this property for $\eta_i(t)$ as defined in (6), the function $g_i(t)$ must be selected according to standard practice in prescribed performance control. Specifically, $g_i(t)$ must be a smoothly monotonic function for all $t \geq 0$, satisfying the boundary conditions $g_i(0) = 1$ and $\lim_{t\to\infty} g_i(t) = 0$. Common choices that satisfy these conditions include $g_i(t) = e^{-kt}$ for some constant $k > 0$. With $g_i(t)$ being monotonically decreasing, its derivative $\frac{dg_i}{dt} \leq 0$. Since we impose $0 < \eta_{i,\infty} < \eta_{i,0} \leq 1$, the term $(\eta_{i,0} - \eta_{i,\infty})$ is strictly positive. Therefore, the derivative $\frac{d\eta_i}{dt} = \left(\eta_{i,0} - \eta_{i,\infty}\right)\frac{dg_i}{dt}$ is guaranteed to be non-positive, confirming the monotonic decrease of $\eta_i(t)$. It is important to emphasize that function $g_i(t)$ which satisfying the boundary conditions but are not monotonically decreasing over the entire domain $t \geq 0$ (such as piecewise functions with initial increasing segments) are not suitable for this framework, as they would lead to non-monotonic behavior in $\eta_i(t)$.

### D. Asymmetric Boundary Function

The asymmetric boundary function can be defined as follows

$$l_{i,1} = \frac{\varsigma_i}{\left(\mu_{i,1}\gamma_{i,1} - \varsigma_i\right)\left(\mu_{i,2}\gamma_{i,2} + \varsigma_i\right)} \tag{12}$$

where $\varsigma_i = \frac{\Phi_{i,1}}{\eta_i(t)}$, and $\Phi_{i,1} = \tanh\left(\frac{e_i}{v_i}\right)$.

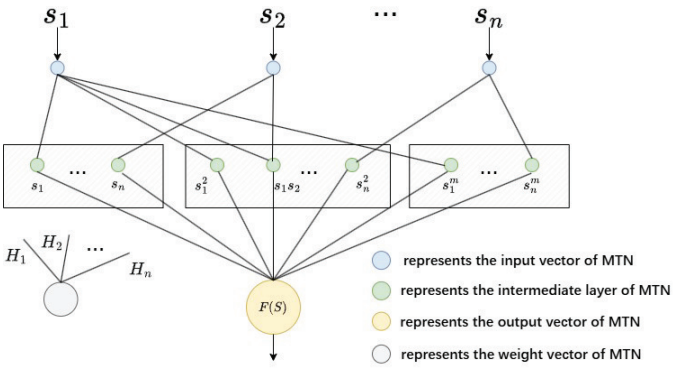


Fig. 1. The structure of MTN.

*Lemma 1 [43]:* If the transformed error function $l_{i,1}$ remains uniformly bounded for all $t \geq 0$, and the initial condition $-\mu_{i,2}\gamma_{i,2}(0) < \varsigma_i(0) < \mu_{i,1}\gamma_{i,1}(0)$ holds, then the synchronization error $e_i$ is guaranteed to adhere to the prescribed performance constraints $-\zeta^*_{i,2} < e_i < \zeta^*_{i,1}$ for all subsequent time $t \geq 0$.

*Remark 2:* To concurrently manage input saturation and output performance constraints, this work develops a performance function framework incorporating an auxiliary boundary function $\zeta\left(\rho_{i,m}(t)\right)$, which is based on a time-varying function $\eta_i(t)$. An associated auxiliary system, defined in (8), is designed utilizing this structure to mitigate the adverse effects of input saturation. Subsequently, the overall performance function dynamically utilizes non-negative signals generated by this auxiliary system, thereby ensuring adherence to the system's output constraints. Distinct from conventional strategies, and as indicated by the auxiliary state dynamics in (9), the proposed method does not modify the performance boundaries based merely on the occurrence of saturation. Instead, a non-negative auxiliary signal is generated, triggering boundary adaptation, only when input saturation occurs and the synchronization error $e_i$ violates the safety margin defined by $\chi_i\zeta\left(\rho_{i,1}(t)\right)$. This conditional adaptation mechanism underscores the flexibility and robustness of the proposed approach in handling coupled constraints.

### E. Multi-Dimensional Taylor Network (MTN)

This study employs MTN for the approximation of unknown nonlinearities inherent within the system dynamics. As a specialized neural architecture, MTN incorporates input, intermediate, and output layers, its structural representation is depicted in Fig. 1.

Foundational details regarding MTN can be found in [44] and [45]. The subsequent *Lemma* formalizes its function approximation capabilities.

*Lemma 2 [44]:* Within a compact set, an unknown smooth nonlinear function $F(\boldsymbol{S}): \Re^n \to \Re$ can be approximated using the MTN formulation

$$F(\boldsymbol{S}) = \boldsymbol{H}^{\mathrm{T}}\boldsymbol{\xi}_{m_n}(\boldsymbol{S}) + \delta(\boldsymbol{S}),\ |\delta(\boldsymbol{S})| \leq \varepsilon \tag{13}$$

where $\boldsymbol{S} = [s_1, s_2, \ldots, s_n]^{\mathrm{T}} \subset \Re^n$ serves as the input vector, and $\boldsymbol{H} = [H_1, H_2, \ldots, H_n]^{\mathrm{T}} \subset \Re^l$ represents the weight vector. $\delta(\boldsymbol{S})$ denotes the approximation error. $\boldsymbol{\xi}_{m_n}(\boldsymbol{S}) = \left[s_1, \ldots, s_n, s_1^2, s_1s_2, \ldots, s_n^2, \ldots, s_1^m, \ldots, s_n^m\right]^{\mathrm{T}}$ represents the intermediate layer of the MTN. $\varepsilon$ is a positive constant.

*Remark 3:* MTN is a specialized neural network architecture, distinguished from conventional networks by its middle layer, which is based on a Taylor series expansion. By leveraging multi-dimensional Taylor expansion, MTN effectively approximates complex nonlinear relationships. Compared to traditional neural networks, MTN exhibits a simpler structure and superior approximation capabilities.

## III. Controller Design and Stability Analysis

### A. Controller Design

In this section, an adaptive MTN-based control scheme is developed for nonlinear multi-agent systems with multiple constraints, incorporating an auxiliary system and a first-order filter.

First, the coordinate transformation is formulated as follows

$$s_{i,1} = l_{i,1} - \phi_{i,1} \tag{14}$$

where $\phi_{i,1}$ represents the auxiliary system signal.

By differentiating $s_{i,1}$ with respect to time, the following result is obtained

$$\dot{s}_{i,1} = m_{i,1}B_ix_{i,2} + m_{i,1}B_i\Delta_{i,1} + W_{i,1} - \dot{\phi}_{i,1} \tag{15}$$

where $\dot{\varsigma}_i = \frac{1}{\eta_i^2}\left(\left(1-\Phi_{i,1}^2\right)\dot{e}_iv_i^{-1}\eta_i - \Phi_{i,1}\dot{\eta}_i\right)$, $\bar{\sigma}_{i,1} = \mu_{i,1}\mu_{i,2}\gamma_{i,1}\gamma_{i,2} + \varsigma_i^2$, $\underline{\sigma}_{i,1} = \left[\left(\mu_{i,1}\gamma_{i,1} - \varsigma_i\right)\left(\mu_{i,2}\gamma_{i,2} + \varsigma_i\right)\right]^2$, $W_{i,1} = m_{i,1}B_iw_{i,1} - m_{i,1}M_i\left(x_{j,2} + w_{j,1}\right) - m_{i,1}M_i\Delta_{j,1} - m_{i,1}b_i\dot{y}_f - \frac{\bar{\sigma}_{i,1}}{\underline{\sigma}_{i,1}}\Phi_{i,1}\frac{\dot{\eta}_i}{\eta_i} - \frac{\varsigma_i\left(\mu_{i,1}\mu_{i,2}\gamma_{i,2}+\mu_{i,1}\varsigma_i\right)\dot{\gamma}_{i,1}}{\underline{\sigma}_{i,1}} - \frac{\varsigma_i\left[\mu_{i,1}\mu_{i,2}\gamma_{i,1}-\mu_{i,2}\varsigma_i\right]\gamma_{i,2}}{\underline{\sigma}_{i,1}} - \frac{\Phi_{i,1}\dot{\eta}_i}{\eta_i^2}$, and $m_{i,1} = \frac{\bar{\sigma}_{i,1}}{\underline{\sigma}_{i,1}}\left(1-\Phi_{i,1}^2\right)\frac{1}{\eta_i}\frac{1}{v_i}$.

*Step 1:* Consider the following formulation for the Lyapunov function $V_{i,1}$

$$V_{i,1} = \frac{1}{2}s_{i,1}^2 + \frac{1}{2}\tilde{\boldsymbol{H}}_{i,1}^T\tilde{\boldsymbol{H}}_{i,1} \tag{16}$$

where $\boldsymbol{H}_{i,1}$ defines the weight vector of the MTN, $\hat{\boldsymbol{H}}_{i,1}$ and $\tilde{\boldsymbol{H}}_{i,1}$ is its estimate. $\tilde{\boldsymbol{H}}_{i,1}$ represents the estimation error of $\boldsymbol{H}_{i,1}$, defined as $\tilde{\boldsymbol{H}}_{i,1} = \boldsymbol{H}_{i,1} - \hat{\boldsymbol{H}}_{i,1}$.

By differentiating $V_{i,1}$ with respect to time, the following is derived

$$\begin{aligned}\dot{V}_{i,1} = s_{i,1}\Big(&m_{i,1}B_i\Big(s_{i,2} + \sigma_{i,2} + \alpha_{i,1} + \phi_{i,2} + \bar{F}_{i,1} \\ &- \frac{3}{2}s_{i,1} + \Delta_{i,1}\Big)\Big) - s_{i,1}m_{i,1}B_i\phi_{i,2} + s_{i,1}k_{i,1}\phi_{i,1} \\ &- \tilde{\boldsymbol{H}}_{i,1}^T\dot{\hat{\boldsymbol{H}}}_{i,1}\end{aligned} \tag{17}$$

where $\bar{W}_{i,1} = W_{i,1} + \frac{3}{2}s_{i,1}$.

According to *Lemma 2*, the approximation of the unknown term $\bar{W}_{i,1}$ is achieved using MTN according to the following structure

$$\bar{W}_{i,1} = \boldsymbol{H}_{i,1}^T\boldsymbol{\xi}_{i,1}(\boldsymbol{Z}) + \delta_{i,1}(\boldsymbol{Z}),\ \left|\delta_{i,1}(\boldsymbol{Z})\right| \leq \varepsilon_{i,1} \tag{18}$$

where $\delta_{i,1}(\boldsymbol{Z})$ is the approximation error of the combination term $\bar{W}_{i,1}$ and $\boldsymbol{H}_{i,1}^T\boldsymbol{\xi}_{i,1}(\boldsymbol{Z})$. $\varepsilon_{i,1} > 0$ is a constant.

The derivation of the following inequalities is facilitated by Young's inequality

$$s_{i,1}m_{i,1}B_i\Delta_{i,1} \le \frac{1}{2}s_{i,1}^2 + \frac{1}{2}m_{i,1}^2B_i^2\bar{\Delta}_{i,1}^2 \tag{19}$$

$$s_{i,1}m_{i,1}B_i\sigma_{i,2} \le \frac{1}{2}s_{i,1}^2 + \frac{1}{2}m_{i,1}^2B_i^2\sigma_{i,2}^2 \tag{20}$$

$$s_{i,1}\bar{W}_{i,1} \le s_{i,1}\boldsymbol{H}_{i,1}^T\boldsymbol{\xi}_{i,1} + \frac{1}{2}s_{i,1}^2 + \frac{1}{2}\varepsilon_{i,1}^2 \tag{21}$$

Then the virtual control signal $\alpha_{i,1}$ can be defined as follows

$$\alpha_{i,1} = \frac{1}{m_{i,1}B_i}\left(-c_{i,1}s_{i,1} - k_{i,1}\phi_{i,1} - \hat{\boldsymbol{H}}_{i,1}^T\boldsymbol{\xi}_{i,1}\right) \tag{22}$$

where $c_{i,1}$ is a positive constant.

The adaptive law $\dot{\hat{\boldsymbol{H}}}_{i,1}$ can be formulated as

$$\dot{\hat{\boldsymbol{H}}}_{i,1} = s_{i,1}\boldsymbol{\xi}_{i,1} - r_{i,1}\hat{\boldsymbol{H}}_{i,1} \tag{23}$$

where $r_{i,1}$ is a positive constant.

A direct derivation using Young's inequality yields the expression that follows

$$r_{i,1}\tilde{\boldsymbol{H}}_{i,1}\hat{\boldsymbol{H}}_{i,1} \le \frac{1}{2}r_{i,1}\left\|H_{i,1}\right\|^2 - \frac{1}{2}r_{i,1}\tilde{\boldsymbol{H}}_{i,1}^T\tilde{\boldsymbol{H}}_{i,1} \tag{24}$$

By combining (19), (20), (21), (22) and (24), the following result can be obtained

$$\begin{aligned}\dot{V}_{i,1} \le& -c_{i,1}s_{i,1}^2 - \frac{1}{2}r_{i,1}\tilde{\boldsymbol{H}}_{i,1}^T\tilde{\boldsymbol{H}}_{i,1} + s_{i,1}m_{i,1}B_is_{i,2}\\ &+ \frac{1}{2}m_{i,1}^2B_i^2(\sigma_{i,2}^2 + \Delta_{i,1}^2) + \frac{1}{2}r_{i,1}\left\|\boldsymbol{H}_{i,1}\right\|^2 + \frac{1}{2}\varepsilon_{i,1}^2\end{aligned} \tag{25}$$

*Step* $j\,(j = 2,\ldots,n-1)$*:* The necessity for differentiation concerning virtual control signals within classical back-stepping frequently leads to the issue referred to as "computational explosion". To avoid this drawback, the derivative of the virtual control signal can be approximated using the output of a first-order filter, thereby preventing the issue of computational explosion.

The approximation is given by

$$\tau_{i,j}\dot{\lambda}_{i,j} = -\lambda_{i,j} + \alpha_{i,j-1} \tag{26}$$

where $j = 2,\ldots,n$. $\tau_{i,j} > 0$ is the time constant. $\lambda_{i,j}$ is the state of the filter with the condition of $\lambda_{i,j}(0) = \alpha_{i,j-1}(0)$.

By differentiating the filter error signal $\sigma_{i,j}$ with respect to time, the following result is derived

$$\dot{\sigma}_{i,j} = \left(-\frac{\sigma_{i,j}}{\tau_{i,j}} + Q_{i,j}\right) \tag{27}$$

where $Q_{i,j} = -\sum_{o=1}^{j-1}\frac{\partial\alpha_{i,j}}{\partial x_{i,o}}\dot{x}_{i,o} - \sum_{o=1}^{j-1}\frac{\partial\alpha_{i,j}}{\partial x_{j,r}}\dot{x}_{j,r} - \sum_{o=1}^{j-1}\frac{\partial\alpha_{i,j}}{\partial\hat{\boldsymbol{H}}_{i,o}}\dot{\hat{\boldsymbol{H}}}_{i,o} - \sum_{o=1}^{j-1}\frac{\partial\alpha_{i,j}}{\partial\phi_{i,o}}\dot{\phi}_{i,o} - \sum_{o=2}^{j-1}\frac{\partial\alpha_{i,j}}{\partial\lambda_{i,o}}\dot{\lambda}_{i,o}$.

Since $Q_{i,j}$ can be derived from the partial derivative of the virtual control signal $\alpha_{i,j}$, and the signal $Q_{i,j}$ is continuous and bounded with the condition $\left|Q_{i,j}\right| \le \bar{Q}_{i,j}$, $\bar{Q}_{i,j} > 0$ is treated as a constant, as discussed in [46].

The coordinate transformation is proposed as follows

$$\begin{cases} s_{i,j} = x_{i,j} - \lambda_{i,j} - \phi_{i,j} \\ \sigma_{i,j} = \lambda_{i,j} - \alpha_{i,j-1},\ j = 2,\ldots,n \end{cases} \tag{28}$$

where $\lambda_{i,j}$ is the output signal of the filter. $\alpha_{i,j-1}$ represents the virtual control signal that will be designed later. $\sigma_{i,j}$ represents the filter error.

Consider the following formulation for the Lyapunov function $V_{i,j}$

$$V_{i,j} = V_{i,j-1} + \frac{1}{2}s_{i,j}^2 + \frac{1}{2}\sigma_{i,j}^2 + \frac{1}{2}\tilde{\boldsymbol{H}}_{i,j}^T\tilde{\boldsymbol{H}}_{i,j} \tag{29}$$

where $\boldsymbol{H}_{i,j}$ defines the weight vector of the MTN, and $\hat{\boldsymbol{H}}_{i,j}$ is its estimate. $\tilde{\boldsymbol{H}}_{i,j}$ represents the estimation error of $\boldsymbol{H}_{i,j}$, defined as $\tilde{\boldsymbol{H}}_{i,j} = \boldsymbol{H}_{i,j} - \hat{\boldsymbol{H}}_{i,j}$.

By differentiating $V_{i,j}$ with respect to time, the following is derived

$$\begin{aligned}\dot{V}_{i,j} =& \dot{V}_{i,j-1} + s_{i,j}\big(s_{i,j+1} + \sigma_{i,j+1} + \alpha_{i,j} + \bar{F}_{i,j}\\ &- s_{i,j}\dot{\lambda}_{i,j} - \frac{3}{2}s_{i,j} + \Delta_{i,j} + k_{i,j}\phi_{i,j}\big)\\ &+ \sigma_{i,j}\left(-\frac{\sigma_{i,j}}{\tau_{i,j}} + Q_{i,j}\right) - \tilde{\boldsymbol{H}}_{i,j}^T\dot{\hat{\boldsymbol{H}}}_{i,j}\end{aligned} \tag{30}$$

where $\bar{W}_{i,j} = w_{i,j} + \frac{3}{2}s_{i,j}$.

According to *Lemma 2*, MTN is employed to approximate the unknown function $\bar{W}_{i,j}$ as follows

$$\bar{W}_{i,j} = \boldsymbol{H}_{i,j}^T\boldsymbol{\xi}_{i,j}(\boldsymbol{Z}) + \delta_{i,j}(\boldsymbol{Z}),\ \left|\delta_{i,j}(\boldsymbol{Z})\right| \le \varepsilon_{i,j} \tag{31}$$

where $\delta_{i,j}(\boldsymbol{Z})$ is the approximation error of the combination term $\bar{W}_{i,j}$ and $\boldsymbol{H}_{i,j}^T\boldsymbol{\xi}_{i,j}(\boldsymbol{Z})$. $\varepsilon_{i,j} > 0$ is a constant.

The derivation of the following inequalities is facilitated by Young's inequality

$$s_{i,j}\sigma_{i,j+1} \le \frac{1}{2}s_{i,j}^2 + \frac{1}{2}\sigma_{i,j+1}^2 \tag{32}$$

$$s_{i,j}\Delta_{i,j} \le \frac{1}{2}s_{i,j}^2 + \frac{1}{2}\bar{\Delta}_{i,j}^2 \tag{33}$$

$$\sigma_{i,j}Q_{i,j} \le \frac{1}{2a_{i,j}^2} + \frac{1}{2}a_{i,j}^2\sigma_{i,j}^2\bar{Q}_{i,j}^2 \tag{34}$$

$$s_{i,j}\bar{W}_{i,j} \le s_{i,j}\boldsymbol{H}_{i,j}^T\boldsymbol{\xi}_{i,j} + \frac{1}{2}s_{i,j}^2 + \frac{1}{2}\varepsilon_{i,j}^2 \tag{35}$$

Then the virtual control signal $\alpha_{i,j}$ can be defined as follows

$$\alpha_{i,j} = -c_{i,j}s_{i,j} - \hat{\boldsymbol{H}}_{i,j}^T\boldsymbol{\xi}_{i,j} - k_{i,j}\phi_{i,j} - P_{i,j}s_{i,j-1} + \dot{\lambda}_{i,j} \tag{36}$$

where $c_{i,j}$ is a positive constant, and $P_{i,j} = \begin{cases} m_{i,1}B_i,\ j = 2 \\ 1,\ j = 3,\ldots,n-1. \end{cases}$

The adaptive law $\dot{\hat{\boldsymbol{H}}}_{i,j}$ can be formulated as

$$\dot{\hat{\boldsymbol{H}}}_{i,j} = s_{i,j}\boldsymbol{\xi}_{i,j} - r_{i,j}\hat{\boldsymbol{H}}_{i,j} \tag{37}$$

where $r_{i,j}$ is a positive constant.

The derivation of the following inequalities is facilitated by Young's inequality

$$r_{i,j}\tilde{\boldsymbol{H}}_{i,j}\hat{\boldsymbol{H}}_{i,j} \le \frac{1}{2}r_{i,j}\left\|\boldsymbol{H}_{i,j}\right\|^2 - \frac{1}{2}r_{i,j}\tilde{\boldsymbol{H}}_{i,j}^T\tilde{\boldsymbol{H}}_{i,j} \tag{38}$$

By combining (32), (33), (34), (36), and (38), it can be derived that

$$\dot{V}_{i,j} \le -\sum_{o=1}^{j}c_{i,o}s_{i,o}^2 - \frac{1}{2}\sum_{o=1}^{j}r_{i,o}\tilde{\boldsymbol{H}}_{i,o}^T\tilde{\boldsymbol{H}}_{i,o} + \frac{1}{2}\sum_{o=2}^{j}a_{i,o}^2$$

$$+\frac{1}{2}\sum_{o=1}^{j}\varepsilon_{i,o}^{2}-\sum_{o=2}^{j}\left(\frac{1}{\tau_{i,j}}-\frac{1}{2}a_{i,o}^{2}\bar{Q}_{i,o}^{2}\right)\sigma_{i,j}^{2}+\frac{1}{2}\sum_{o=1}^{j}\bar{\Delta}_{i,o}^{2}$$
$$+\frac{1}{2}\sum_{o=1}^{j}\sigma_{i,o+1}^{2}+\frac{1}{2}\sum_{o=1}^{j}r_{i,o}\left\|\boldsymbol{H}_{i,o}\right\|^{2}+s_{i,j}s_{i,j+1} \tag{39}$$

*Step n:* By differentiating the filter error signal $\sigma_{i,n}$ with respect to time, the following result is derived

$$\dot{\sigma}_{i,n}=\left(-\frac{\sigma_{i,n}}{\tau_{i,n}}+Q_{i,n}\right) \tag{40}$$

where $Q_{i,n}=-\sum_{o=1}^{n-1}\frac{\partial\alpha_{i,j}}{\partial x_{i,o}}\dot{x}_{i,o}-\sum_{o=1}^{n-1}\frac{\partial\alpha_{i,j}}{\partial x_{j,r}}\dot{x}_{j,r}-\sum_{o=1}^{n-1}\frac{\partial\alpha_{i,j}}{\partial\hat{\boldsymbol{H}}_{i,o}}\dot{\hat{\boldsymbol{H}}}_{i,o}-\sum_{o=1}^{n-1}\frac{\partial\alpha_{i,j}}{\partial\phi_{i,o}}\dot{\phi}_{i,o}-\sum_{o=2}^{n-1}\frac{\partial\alpha_{i,j}}{\partial\lambda_{i,o}}\dot{\lambda}_{i,o}$.

Since $Q_{i,n}$ can be derived from the partial derivative of $\alpha_{i,n-1}$, and $Q_{i,n}$ is continuous and bounded satisfying $\left|Q_{i,n}\right|\leq\bar{Q}_{i,n}$, $\bar{Q}_{i,n}>0$ is a constant, as discussed in [46].

Consider the following formulation for the Lyapunov function $V_{i,n}$

$$V_{i,n}=V_{i,n-1}+\frac{1}{2}s_{i,n}^{2}+\frac{1}{2}\sigma_{i,n}^{2}+\frac{1}{2}\tilde{\boldsymbol{H}}_{i,n}^{T}\tilde{\boldsymbol{H}}_{i,n} \tag{41}$$

where $\boldsymbol{H}_{i,n}$ defines the weight vector of MTN, and $\hat{\boldsymbol{H}}_{i,n}$ is its estimate. $\tilde{\boldsymbol{H}}_{i,n}$ represents the estimation error of $\boldsymbol{H}_{i,n}$, defined as $\tilde{\boldsymbol{H}}_{i,n}=\boldsymbol{H}_{i,n}-\hat{\boldsymbol{H}}_{i,n}$.

By differentiating $V_{i,n}$ with respect to time, we have

$$\dot{V}_{i,n}=\dot{V}_{i,n-1}+s_{i,n}\big(u_{i}+\bar{F}_{i,n}-s_{i,n-1}-s_{i,n}+\Delta_{i,n}-\dot{\lambda}_{i,n}+k_{i,n}\phi_{i,n}\big)+\sigma_{i,n}\left(-\frac{\sigma_{i,n}}{\tau_{i,n}}+Q_{i,n}\right)-\tilde{\boldsymbol{H}}_{i,n}^{T}\dot{\hat{\boldsymbol{H}}}_{i,n} \tag{42}$$

where $\bar{W}_{i,n}=w_{i,n}+s_{i,n}$ is a combination of nonlinear functions.

According to Lemma 2, the approximation of the unknown term $\bar{W}_{i,n}$ is achieved using MTN according to the following structure

$$\bar{W}_{i,n}=\boldsymbol{H}_{i,n}^{T}\boldsymbol{\xi}_{i,n}(\boldsymbol{Z})+\delta_{i,n}(\boldsymbol{Z}),\ \left|\delta_{i,n}(\boldsymbol{Z})\right|\leq\varepsilon_{i,n} \tag{43}$$

where $\delta_{i,n}(\boldsymbol{Z})$ is the approximation error of the combination term $\bar{W}_{i,n}$ and $\boldsymbol{H}_{i,n}^{T}\boldsymbol{\xi}_{i,n}(\boldsymbol{Z})$. $\varepsilon_{i,n}>0$ is a constant.

The derivation of the following inequalities is facilitated by Young's inequality

$$s_{i,n}\Delta_{i,n}\leq\frac{1}{2}s_{i,n}^{2}+\frac{1}{2}\bar{\Delta}_{i,n}^{2} \tag{44}$$
$$\sigma_{i,n}Q_{i,n}\leq\frac{1}{2a_{i,n}^{2}}+\frac{1}{2}a_{i,n}^{2}\sigma_{i,n}^{2}\bar{Q}_{i,n}^{2} \tag{45}$$
$$s_{i,n}\bar{W}_{i,n}\leq s_{i,n}\boldsymbol{H}_{i,n}^{T}\boldsymbol{\xi}_{i,n}+\frac{1}{2}s_{i,n}^{2}+\frac{1}{2}\varepsilon_{i,n}^{2} \tag{46}$$

Then the controller $u_i$ can be designed as follows

$$u_{i}=-c_{i,n}s_{i,n}-\hat{\boldsymbol{H}}_{i,n}^{T}\boldsymbol{\xi}_{i,n}-s_{i,n-1}-k_{i,n}\phi_{i,n}+\dot{\lambda}_{i,n} \tag{47}$$

where $c_{i,n}$ is a positive constant.

The adaptive law $\dot{\hat{\boldsymbol{H}}}_{i,n}$ can be formulated as

$$\dot{\hat{\boldsymbol{H}}}_{i,n}=s_{i,n}\boldsymbol{\xi}_{i,n}-r_{i,n}\hat{\boldsymbol{H}}_{i,n} \tag{48}$$

where $r_{i,n}$ is a positive constant.

The derivation of the following inequalities is facilitated by Young's inequality

$$r_{i,n}\tilde{\boldsymbol{H}}_{i,n}\hat{\boldsymbol{H}}_{i,n}\leq\frac{1}{2}r_{i,n}\left\|\boldsymbol{H}_{i,n}\right\|^{2}-\frac{1}{2}r_{i,n}\tilde{\boldsymbol{H}}_{i,n}^{T}\tilde{\boldsymbol{H}}_{i,n} \tag{49}$$

Substituting (44), (45), (46), (47), (49) into (42), the following result can be obtained

$$\dot{V}_{i,n}\leq-\sum_{o=1}^{n}c_{i,o}s_{i,o}^{2}-\sum_{o=2}^{n}\left(\frac{1}{\tau_{i,j}}-\frac{1}{2}a_{i,o}^{2}\bar{Q}_{i,o}^{2}\right)\sigma_{i,j}^{2}-\frac{1}{2}\sum_{o=1}^{n}r_{i,o}\tilde{\boldsymbol{H}}_{i,o}^{T}\tilde{\boldsymbol{H}}_{i,o}+\frac{1}{2}\sum_{o=1}^{n}r_{i,o}\left\|\boldsymbol{H}_{i,o}\right\|^{2}+\frac{1}{2}\sum_{o=1}^{n}(\bar{\Delta}_{i,o}^{2}+\varepsilon_{i,o}^{2})+\frac{1}{2}\sum_{o=1}^{n-1}\sigma_{i,o+1}^{2}+\frac{1}{2}\sum_{o=2}^{n}a_{i,o}^{2} \tag{50}$$

## B. Stability Analysis

*Theorem 1:* By employing the virtual control specifications (22), (36), the actual control computation (47), and the adaptive update laws (23), (37), (48) for the constrained nonlinear multi-agent systems (1)–(2), the following conclusions hold:

i) Guarantee the boundedness of all signals within the closed-loop system.

ii) The synchronization error satisfies the predefined criteria $-\zeta_{i,2}^{*}<e_{i}<\zeta_{i,1}^{*}$.

*Proof:*

i) The final Lyapunov function for the nonlinear multi-agent system is defined as follows

$$V=\sum_{i=1}^{N}\left(\frac{1}{2}\sum_{o=1}^{n}s_{i,o}^{2}+\frac{1}{2}\sum_{o=2}^{n}\sigma_{i,j}^{2}+\frac{1}{2}\sum_{o=1}^{n}\tilde{\boldsymbol{H}}_{i,o}^{T}\tilde{\boldsymbol{H}}_{i,o}\right) \tag{51}$$

As stated in equation (50), we have

$$\dot{V}\leq\sum_{i=1}^{N}\Big(-\sum_{o=1}^{n}c_{i,o}s_{i,o}^{2}-\frac{1}{2}\sum_{o=1}^{n}r_{i,o}\tilde{\boldsymbol{H}}_{i,o}^{T}\tilde{\boldsymbol{H}}_{i,o}-\sum_{o=2}^{n}\left(\frac{1}{\tau_{i,j}}-\frac{1}{2}a_{i,o}^{2}\bar{Q}_{i,o}^{2}\right)\sigma_{i,j}^{2}+\kappa_{i}\Big) \tag{52}$$

where $\kappa_{i}=\frac{1}{2}\sum_{o=1}^{n}r_{i,o}\left\|\boldsymbol{H}_{i,o}\right\|^{2}+\frac{1}{2}\sum_{o=1}^{n}\bar{\Delta}_{i,o}^{2}+\frac{1}{2}\sum_{o=1}^{n-1}\sigma_{i,o+1}^{2}+\frac{1}{2}\sum_{o=1}^{n}\varepsilon_{i,o}^{2}+\frac{1}{2}\sum_{o=2}^{n}a_{i,o}^{2}$ represents a constant.

By combining equations (51) and (52), it follows that

$$\dot{V}\leq-aV+b \tag{53}$$

where $a=\min\left\{2c_{i,o},2\left(\frac{1}{\tau_{i,j}}-\frac{1}{2}a_{i,o}^{2}\bar{Q}_{i,o}^{2}\right),r_{i,o}\right\}$, and $b=\sum_{i=1}^{N}\kappa_{i}$.

By multiplying both sides of the inequality (53) by $e^{-at}$, the following result is obtained

$$V(t)\leq V(0)e^{-at}+\frac{b}{a} \tag{54}$$

Thus, according to equation (54), it is guaranteed the boundedness of all signals within the closed-loop system, then $e_i$ is bounded.

ii) Based on (12), it is known that $\varsigma_{i}=\tanh\left(\frac{e_{i}}{v_{i}}\right)\eta_{i}^{-1}(t)$ is bounded, thus guaranteeing boundedness of $s_{i,1}$. Given that the

initial condition $-\mu_{i,2}\gamma_{i,2}(0) < \varsigma_i(0) < \mu_{i,1}\gamma_{i,1}(0)$ is satisfied, then it follows that $-\mu_{i,2}\gamma_{i,2}(t) < \varsigma_i < \mu_{i,1}\gamma_{i,1}(t)$, and one can deduce that $-\tilde{\rho}_{i,2}(t) < v_{i,1} < \tilde{\rho}_{i,1}(t)$. Based on the properties of the functions $\tilde{\rho}_{i,m}$ and $\zeta^*_{i,m}$, the following conclusion can be made

$$-\zeta^*_{i,2} < e_i < \zeta^*_{i,1} \tag{55}$$

Hence, the *Theorem 1* is proven.

In addition, when the parameters are appropriately selected that $\mu_{i,1} = \mu_{i,2} = \eta_{i,0} = 1$, the calculations yield $\gamma_{i,1} = \gamma_{i,2} = 1$, then $\tilde{\rho}_{i,1} = \eta_i(0)\mu_{i,1}\gamma_{i,1} = 1$, $\tilde{\rho}_{i,2} = \eta_i(0)\mu_{i,2}\gamma_{i,2} = 1$. By calculating $\zeta^*_{i,m}$, we can easily conclude that

$$\begin{cases} \zeta^*_{i,1} = \dfrac{v_i}{2}\ln\dfrac{1+\tilde{\rho}_{i,1}}{1-\tilde{\rho}_{i,1}} \to +\infty \\ -\zeta^*_{i,2} = \dfrac{v_i}{2}\ln\dfrac{1+\tilde{\rho}_{i,2}}{1-\tilde{\rho}_{i,2}} \to -\infty \end{cases} \tag{56}$$

According to (56), for all $t > 0$, the following inequality holds

$$-\infty < -\zeta^*_{i,2}(0) < e_i(0) < \zeta^*_{i,1}(0) < +\infty \tag{57}$$

Thus, the system achieves global performance based on its dynamics.

*Remark 4:* The auxiliary system, theoretically defined by dynamics such as those in (3), (8), and (9), serves the crucial functions of compensating for input saturation effects and enabling dynamic adjustment of performance boundaries within the nonlinear multi-agent control framework. Facilitating its practical deployment necessitates several considerations. Firstly, For practical deployment on digital control platforms typical in multi-agent applications like UAV swarms or sensor networks, the continuous-time dynamics of the auxiliary system require discretization, standard numerical integration techniques such as the Euler method can readily convert the defining differential equations into suitable difference equations. Secondly, The inherent structural simplicity of the proposed auxiliary system, generally involving first-order dynamics and straightforward logic, ensures computational tractability and facilitates real-time execution even on resource-constrained embedded processors. Effective performance hinges on the appropriate selection and tuning of auxiliary system parameters, a process typically involving simulation and empirical adjustment based on specific system characteristics to achieve the desired balance between responsiveness and stability, as elaborated upon concerning parameter roles in Remark 5. Finally, the integration of the auxiliary system into the existing control architecture is straightforward. It primarily utilizes readily available signals, such as the control input $u_i$ and the saturation error $\Delta u_i = p_i(u_i) - u_i$, without necessitating additional hardware sensors. The feasibility of this approach, including successful parameter tuning for robust operation under coupled constraints, is substantiated by the simulation results involving single-link robotic arms presented in Section IV, affirming the practical applicability and robust performance of the overall control strategy under input and output constraints.

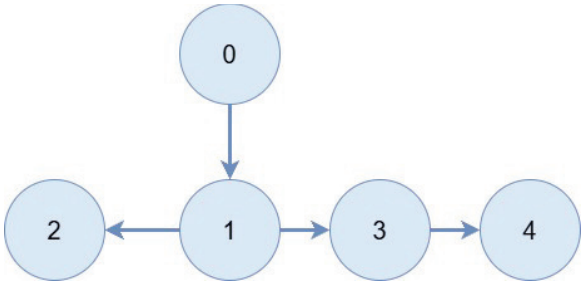


Fig. 2. Communication topology.

## IV. Simulation Results

In this section, two Examples are presented to demonstrate the feasibility and effectiveness of the adaptive MTN proposed in this paper.

### A. Numerical Example

Consider a leader-follower architecture involving four followers, where each agent exhibits second-order nonlinear dynamics. The communication graph for this system, represented in Fig. 2, fulfills the requirements specified under Assumption 2.

The communication topology among the agents is shown in Fig. 2.

From Fig. 2, we define the Laplacian matrix $\mathcal{L} = \begin{pmatrix} 0 & 0 & 0 & 0 \\ -1 & 1 & 0 & 0 \\ -1 & 0 & 1 & 0 \\ 0 & 0 & -1 & 1 \end{pmatrix}$.

The dynamics of the follower agents are governed by the following equation

$$\begin{cases} \dot{x}_{i,1} = x_{i,2} - 0.5x_{i,1} \\ \dot{x}_{i,2} = p_i(u_i) - x_{i,2} - \sin\left(x_{i,1}\right) + \Delta_i(t) \\ y_i = x_{i,1}, i = 1,2,3,4 \end{cases} \tag{58}$$

where $p_i(u_i)$ represents the saturation function, and the corresponding control input and system output are respectively denoted by $u_i \in \mathfrak{R}$ and $y_i \in \mathfrak{R}$. $\Delta_i(t)$ is the external disturbance.

The external disturbance is defined as $\Delta_i(t) = c\epsilon_i \sin(t)$, where $\epsilon_i$ and $c$ are constants and satisfy $\epsilon_1 = 3.5$, $\epsilon_2 = 3.03$, $\epsilon_3 = 3.3$, $\epsilon_4 = 0.3$, and $\begin{cases} c = 0, t < 10 \\ c = 1, t \geq 10 \end{cases}$.

The leader agent generates the reference signal according to $y_f = \sin(t)$. The formulation for the asymmetric input saturation nonlinearity is defined as

$$p_i(u_i) = \begin{cases} -5, & u_i < -5 \\ u_i, & -5 \leq u_i \leq 3 \\ 3, & u_i > 3 \end{cases} \tag{59}$$

The time-varying function is chosen as

$$g_i(t) = \begin{cases} \left(\dfrac{3-t}{3}\right)^2, & 0 \leq t \leq 3 \\ 0, & t > 3 \end{cases} \tag{60}$$

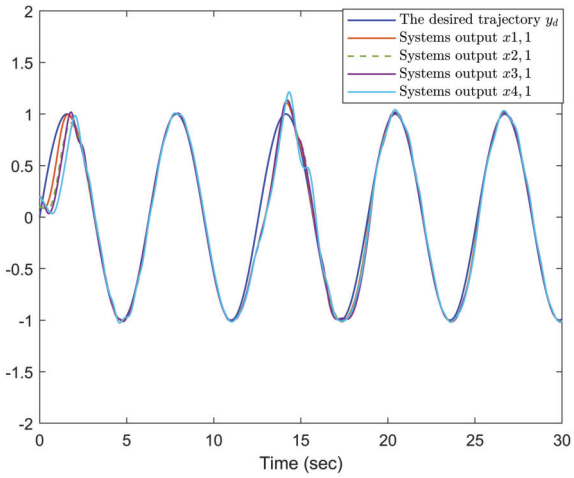


Fig. 3. Leader-follower tracking signals.

The parameters of the time-varying function are chosen as $\eta_{1,0} = \eta_{2,0} = \eta_{3,0} = 1$, $\eta_{4,0} = 1$, and $\eta_{1,\infty} = \eta_{2,\infty} = \eta_{3,\infty} = 0.1$, $\eta_{4,\infty} = 0.1$, which ensure that

$$\eta_i(t) = 0.9\left(\frac{3-t}{3}\right)^2 + 0.1 \tag{61}$$

The parameters for the auxiliary system addressing input saturation are $k_{1,1} = k_{2,1} = 3$, $k_{1,2} = 2.5$, $k_{2,2} = 10$, $k_{3,1} = 4$, $k_{3,2} = k_{4,1} = 8$,, $k_{4,2} = 2$, $b_{1,1,1} = b_{1,2,1} = 1$, $b_{2,1,1} = b_{2,2,1} = b_{3,1,1} = b_{3,2,1} = b_{4,1,1} = b_{4,2,1} = 0.1$, $d_{1,1,1} = 1$, $d_{1,2,1} = 0.5$, $d_{2,1,1} = 2$, $d_{2,2,1} = d_{3,1,1} = d_{3,2,1} = 10$, $d_{4,1,1} = d_{4,2,1} = 1$, $\chi_1 = \chi_2 = \chi_3 = \chi_4 = 0.6$. Parameters in the boundary and asymmetric barrier functions are chosen as $v_1 = v_2 = v_3 = v_4 = 1$, $\mu_{1,1} = \mu_{1,2} = 1$, $\mu_{2,1} = \mu_{2,2} = 0.8$, $\mu_{3,1} = 0.8$, $\mu_{3,2} = 1$, $\mu_{4,1} = \mu_{4,2} = 1$, $R_{1,1} = R_{1,2} = R_{2,1} = R_{2,2} = R_{3,1} = R_{3,2} = 3$, $a_{1,1} = a_{1,2} = a_{2,1} = a_{2,2} = a_{3,1} = a_{3,2} = a_{4,1} = a_{4,2} = 1$, $R_{4,1} = R_{4,2} = 3$. The parameters for the virtual control law and controller are set to $c_{1,1} = 7$, $c_{2,1} = 11$, $c_{3,1} = 18$, $c_{4,1} = 10$, $c_{1,2} = 60$, $c_{2,2} = 20$, $c_{3,2} = 40$, $c_{4,2} = 400$, while the adaptive law uses $r_{1,1} = r_{1,2} = r_{2,1} = r_{2,2} = r_{3,1} = r_{3,2} = 1$, $r_{4,1} = r_{4,2} = 1$. The time constant for the filter is set to $\tau_{1,1} = \tau_{2,1} = \tau_{3,1} = 1$, $\tau_{4,1} = 1$. The initial states of MASs are chosen as: $\bar{x}_{1,2}(\mathbf{0}) = \left[x_{1,1}(0), x_{1,2}(0)\right] = [0.1, 0]^{\mathrm{T}}$, $\bar{x}_{2,2}(\mathbf{0}) = \left[x_{2,1}(0), x_{2,2}(0)\right] = [0.1, 0]^{\mathrm{T}}$, $\bar{x}_{3,2}(\mathbf{0}) = \left[x_{3,1}(0), x_{3,2}(0)\right] = [0.2, 0.1]^{\mathrm{T}}$, $\bar{x}_{4,2}(\mathbf{0}) = \left[x_{4,1}(0), x_{4,2}(0)\right] = [0.2, 0]^{\mathrm{T}}$. By combining the virtual control laws (22) and (36), the control law (47), the adaptive laws (23), (37), (48), and the filters (26), (40), it is ensured that the boundedness of all signals within the closed-loop system.

The simulation results are presented in Figs. 3–6. Fig. 3 demonstrates that each agent rapidly tracks the reference signal, leading to system consensus. Upon the introduction of disturbances, the system quickly adjusts and continues to accurately track the reference signal. Figs. 4 demonstrate that the synchronization error for each agent consistently remains within the predefined boundary. At specific time, when the system experiences external disturbances, the proposed performance function adjusts automatically. As the synchronization error increases, the constraint range is preemptively adjusted,

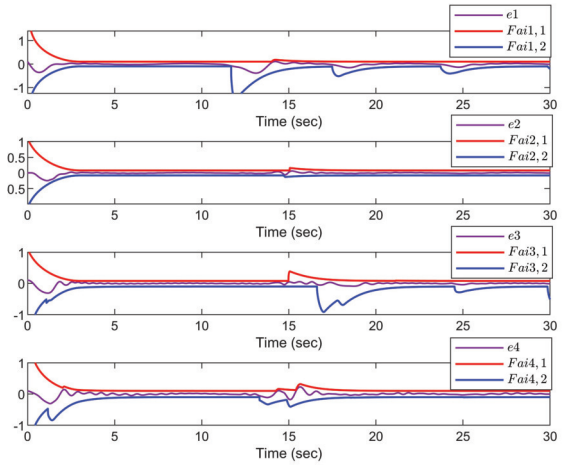


Fig. 4. Output constraint of agents 1-4.

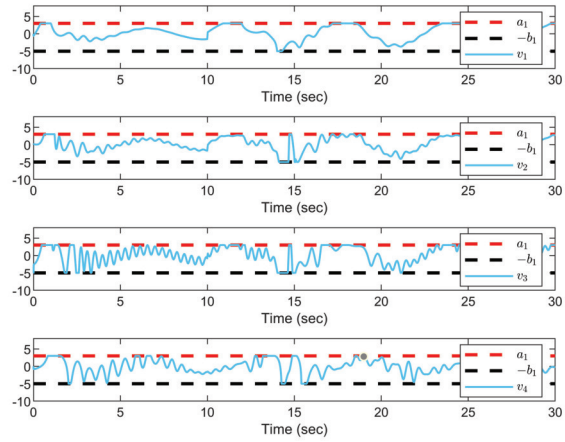


Fig. 5. Input saturation for agents 1-4.

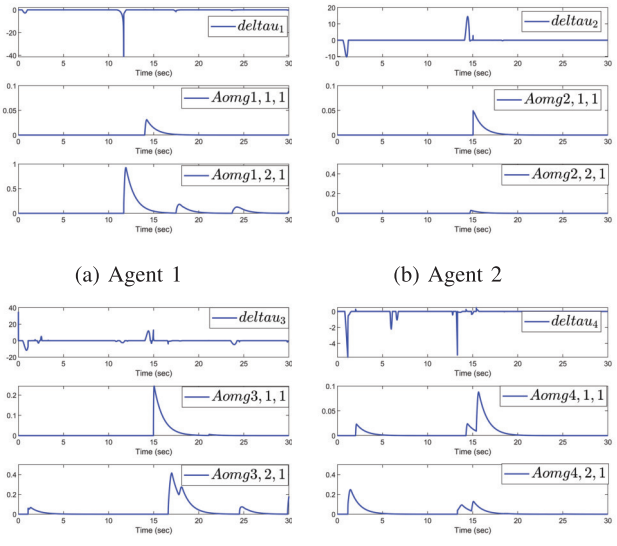


(a) Agent 1 (b) Agent 2

(c) Agent 3 (d) Agent 4

Fig. 6. Non-negative auxiliary signal generated by the auxiliary system for agent 1-4.

ensuring the error remains within the prescribed boundary. Fig. 5 illustrates the control inputs for each agent under input

saturation. Fig. 6 demonstrates that, under input saturation, when the synchronization error remains within the performance boundary, a zero-valued auxiliary signal is generated. In the presence of minor disturbances, the proposed control scheme ensures the synchronization error remains within the predefined boundary. When stronger disturbances arise, the designed auxiliary system promptly generates a non-negative signal to adjust the constraint range of the performance function, thereby enforcing multiple constraints within the nonlinear multi-agent system. This highlights the distinction between the proposed method and existing approaches in the literature. The simulation results demonstrate that, under both input and output constraints, the proposed control scheme enables each agent in the nonlinear multi-agent system to rapidly track the reference signal and achieve consensus.

### B. Practical Example

In this section, the practical applicability of the proposed control scheme is substantiated using four single-link robotic manipulators.

$$\begin{cases} \dot{v}_i = q_i \\ M_i \ddot{q}_i + km_i g l_i \sin(q_i) = p_i(u_i) + \Delta_i(t) \\ i = 1, 2, 3, 4 \end{cases} \tag{62}$$

where $k = 0.5$. $M = 1kg * m^2$ represents the moment of inertia, $m_i = 1kg$ is the mass, and $l_i = 1m$ is the length of the robotic arm. The gravitational acceleration is denoted by $g = 9.8m/s^2$, and the angular displacement, velocity, and acceleration of each link are represented by $q_i, \dot{q}_i, \ddot{q}_i$ respectively. The saturation function is denoted by $p_i(u_i)$, and $\Delta_i(t)$ represents external disturbances. Additionally, the communication topology among agents, the leader's reference signal, and the time-varying function are the same as those in the numerical example.

The formulation for the asymmetric input saturation nonlinearity is defined as

$$p_i(u_i) = \begin{cases} -6, & u_i < -6 \\ u_i, & -6 \le u_i \le 4 \\ 4, & u_i > 4 \end{cases} \tag{63}$$

The external disturbance is given by $\Delta_i(t) = c\epsilon_i \sin(t)$, where $\epsilon_i$ and $c$ are constants and satisfy $\epsilon_1 = 7$, $\epsilon_2 = 7.1$, $\epsilon_3 = 6.8$, $\epsilon_4 = 6$, and $\begin{cases} c = 0, t < 10 \\ c = 1, t \ge 10 \end{cases}$.

The parameters for the auxiliary system addressing input saturation are selected as $k_{1,1} = k_{3,2} = k_{4,2} = 10$, $k_{1,2} = k_{4,1} = 2$, $k_{2,1} = 4$, $k_{2,2} = 9$, $k_{3,1} = 5$, $b_{1,1,1} = b_{1,2,1} = 1$, $b_{2,1,1} = b_{2,2,1} = b_{3,1,1} = b_{3,2,1} = 1$, $b_{4,1,1} = b_{4,2,1} = 1$, $d_{1,1,1} = 0.1$, $d_{1,2,1} = 0.05$, $d_{2,1,1} = d_{2,2,1} = d_{3,1,1} = d_{3,2,1} = 1$, $d_{4,1,1} = d_{4,2,1} = 1$, $\chi_1 = \chi_2 = \chi_3 = 0.6$, $\chi_4 = 0.6$, $a_{1,1} = a_{1,2} = a_{2,1} = a_{2,2} = a_{3,1} = a_{3,2} = a_{4,1} = a_{4,2} = 1$, while the parameters for the boundary and asymmetric barrier functions are selected as $v_1 = v_2 = v_3 = 1$, $v_4 = 1$, $\mu_{1,1} = \mu_{1,2} = 1$, $\mu_{2,1} = 0.8$, $\mu_{3,1} = 1$, $\mu_{3,2} = 1$, $\mu_{4,1} = \mu_{4,2} = 1$, $R_{1,1} = 6$, $R_{1,2} = 1$, $R_{2,1} = 4$, $R_{2,2} = 3$, $R_{3,1} = 3$, $R_{3,2} = 2$, $R_{4,1} = R_{4,2} = 3$ and so on. The parameters in the virtual control law and controller are $c_{1,1} = 45$, $c_{2,1} = 8$, $c_{3,1} = 13$, $c_{4,1} = 10$, and the adaptive law uses $c_{1,2} = 40$, $c_{2,2} = 20$, $c_{3,2} = 40$, $c_{4,2} = 400$. The time constant for the filter is set to $\tau_{1,1} = \tau_{2,1} = \tau_{3,1} = 1$, $\tau_{4,1} = 10$.

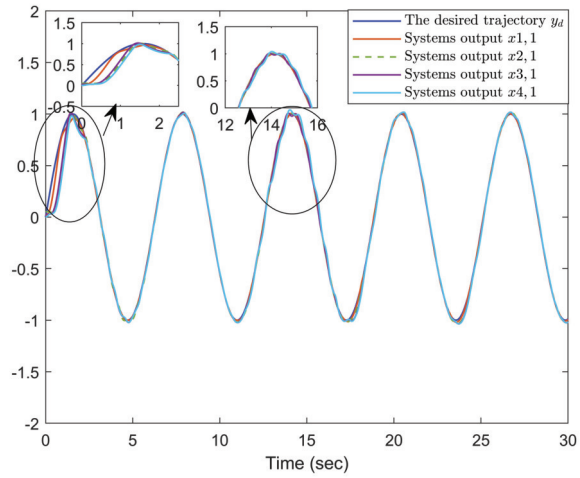


Fig. 7. Leader-follower tracking signals.

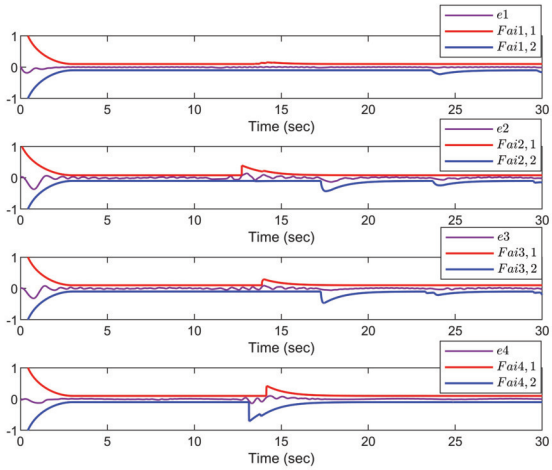


Fig. 8. Output constraint of agents 1-4.

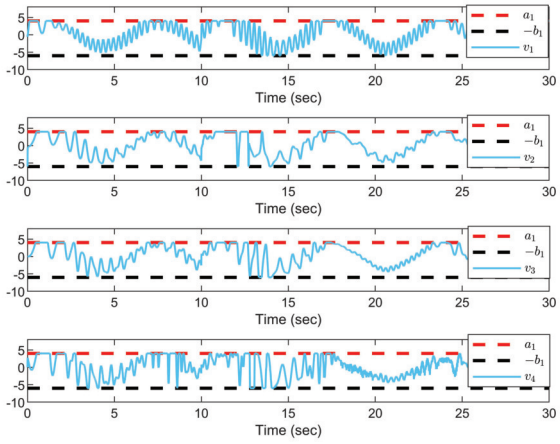


Fig. 9. Input saturation for agents 1-4.

The simulation results are presented in Figs. 7–10. Fig. 7 demonstrates that the system states rapidly track the reference

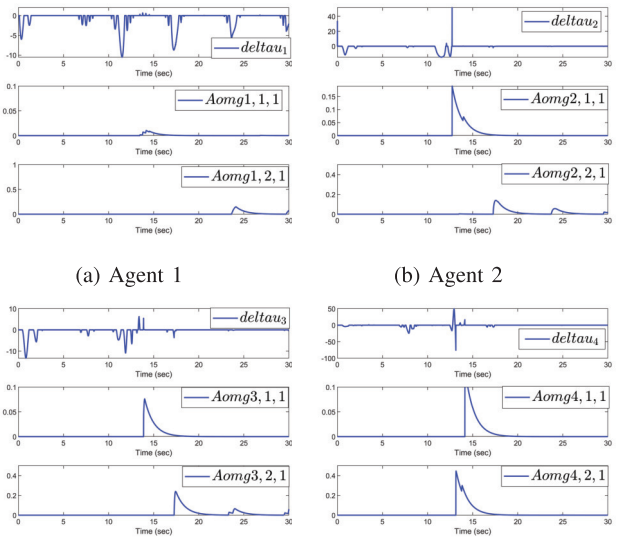


(a) Agent 1 (b) Agent 2

(c) Agent 3 (d) Agent 4

Fig. 10. Non-negative auxiliary signal generated by the auxiliary system for agent 1-4.

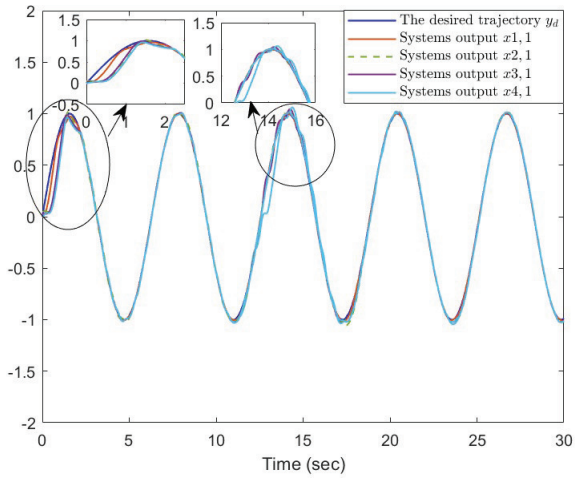


Fig. 11. Tracking curve using RBFNN approximation.

signal. Fig. 8 shows that the synchronization error for each agent consistently remains within the prescribed boundary. Fig. 9 illustrates the control inputs for each agent under input saturation conditions. Fig. 10 presents the non-negative auxiliary signals generated by the auxiliary system for each agent. These results demonstrate that, despite input saturation and output constraints in the nonlinear multi-agent system, the proposed control scheme ensures robust tracking performance and exhibits strong disturbance rejection capabilities.

Additionally, to further elucidate the performance characteristics of the multi-dimensional Taylor network (MTN) relative to conventional neural network approximators within the proposed control framework, the system's tracking performance is compared when employing MTN versus Radial Basis Function Neural Network (RBFNN) for approximating the unknown nonlinearities under identical system conditions and controller architecture (excluding the function approximator itself). The simulation results are depicted in Fig. 7 and Fig. 11. A comparison of the results presented in Fig. 7 and Fig. 11 reveals that while both the MTN-based and RBFNN-based controllers yield comparable tracking performance during the initial phase, a discernible difference emerges following the introduction of disturbances at $t = 10s$. Specifically, within this simulation instance, the nonlinear multi-agent system utilizing MTN maintained robust and accurate tracking performance despite the disturbances. Conversely, under the same disturbance conditions, the system employing the RBF NN exhibited minor oscillations in its tracking trajectory. Consequently, within this specific simulation scenario, the controller incorporating MTN demonstrated superior robustness, potentially highlighting the practical advantages conferred by MTN's structure and approximation capabilities for this particular application.

*Remark 5:* Although the proposed control framework involves numerous design parameters, their inclusion serves to enhance system performance rather than to complicate implementation. Specifically, the controller gains $c_{i,j}$ in the virtual (22), (36)and actual control laws (47) adjust the feedback on the tracking errors $e_{i,j}$, increasing $c_{i,j}$ accelerates convergence and responsiveness but may amplify control effort, exacerbate input saturation, and induce oscillations; decreasing $c_{i,j}$ smooths control actions at the expense of slower tracking and disturbance rejection. The adaptive gains $r_{i,j}$ in the MTN weight update laws (23), (37), (48) regulate adaptation speed. Increasing $r_{i,j}$ expedites weight convergence and improves transient response but risks high frequency oscillations under disturbance, whereas decreasing $r_{i,j}$ enhances robustness yet slows compensation of nonlinearities. The filter time constants $\tau_{i,j}$ in the first order approximations (26), (40) set the trade off between smoothing and responsiveness, larger $\tau_{i,j}$ increases phase lag and filtering, while smaller $\tau_{i,j}$ reduces lag and better tracks the virtual control derivative at the cost of reduced noise attenuation. The dynamic performance function parameters $\eta_{i,0}$, $\eta_{i,\infty}$, $v_i$, $\mu_{i,m}$, $\chi_i$, $R_{i,m}$ in (6)–(11) define the transient error envelope $\eta_{i,0}$ and $\eta_{i,\infty}$ set the initial and final steady-state error bounds, $\mu_{i,m}$ controls the decay rate, $v_i$ scales the barrier steepness, $R_{i,m}$ adjusts boundary expansion gain, and $\chi_i$ specifies the triggering threshold. Finally, the auxiliary system parameters $k_{i,j}$, $b_{i,m,j}$, $d_{i,m,j}$, $m_{i,1}$ in (3), (8), (9) dictate the compensation dynamics for input saturation and performance-triggered events, decay rates $k_{i,j}$, $b_{i,m,j}$ determine reset speed of auxiliary states, while gains $d_{i,m,j}$, $m_{i,1}$ regulate compensation strength. In practice, these parameters should first satisfy the Lyapunov based stability conditions and then be fine tuned via simulation to balance convergence speed, robustness, and implementation feasibility for the target multi agent application.

## V. Conclusion

This paper successfully addresses the adaptive tracking control problem for nonlinear multi-agent systems subject to concurrent input saturation and output performance constraints. A novel control framework is proposed featuring a Dynamic Performance Function (DPF) that implements a precise, conditional adaptation strategy. This strategy adjusts

performance boundaries only when input saturation occurs concurrently with synchronization errors exceeding predefined safety limits, thereby offering targeted conflict resolution without unnecessary performance compromise. This DPF is synergistically integrated with a tailored auxiliary system for asymmetric saturation compensation, providing a unified mechanism for managing the coupled constraints. Furthermore, computational tractability and effective handling of system nonlinearities are achieved by incorporating multi-dimensional Taylor network (MTN) and first-order filter within a backstepping design. Rigorous Lyapunov analysis establishes the boundedness of all closed-loop signals. Simulation results corroborate the framework's effectiveness, demonstrating robust synchronization performance and stability under these challenging multiple constraints.

Future research avenues include investigating scenarios involving communication constraints or cyber-attacks within the multi-agent systems. Furthermore, by extending the control strategy proposed herein, future work will explore its application to stochastic multi-agent systems and fractional-order multi-agent systems under concurrent dual constraints.

## REFERENCES


[1] E. Oliveira, K. Fischer, and O. Stepankova, "Multi-agent systems: Which research for which applications," *Robot. Auto. Syst.*, vol. 27, nos. 1–2, pp. 91–106, Apr. 1999.

[2] Q.-Y. Yu, W.-X. Meng, M.-C. Yang, L.-M. Zheng, and Z.-Z. Zhang, "Virtual multi-beamforming for distributed satellite clusters in space information networks," *IEEE Wireless Commun.*, vol. 23, no. 1, pp. 95–101, Feb. 2016.

[3] S. D. J. McArthur et al., "Multi-agent systems for power engineering applications—Part I: Concepts, approaches, and technical challenges," *IEEE Trans. Power Syst.*, vol. 22, no. 4, pp. 1743–1752, Nov. 2007.

[4] Y. Li and C. Tan, "A survey of the consensus for multi-agent systems," *Syst. Sci. Control Eng.*, vol. 7, no. 1, pp. 468–482, 2019.

[5] J. Qin, Q. Ma, Y. Shi, and L. Wang, "Recent advances in consensus of multi-agent systems: A brief survey," *IEEE Trans. Ind. Electron.*, vol. 64, no. 6, pp. 4972–4983, Jun. 2016.

[6] T. F. Liu and Z.-P. Jiang, "Distributed output-feedback control of nonlinear multi-agent systems," *IEEE Trans. Autom. Control*, vol. 58, no. 11, pp. 2912–2917, Nov. 2013.

[7] X. F. Zhang, L. Liu, and G. Feng, "Leader–follower consensus of time-varying nonlinear multi-agent systems," *Automatica*, vol. 52, pp. 8–14, Feb. 2015.

[8] W. Wu and S. C. Tong, "Fuzzy adaptive consensus control for nonlinear multiagent systems with intermittent actuator faults," *IEEE Trans. Cybern.*, vol. 53, no. 5, pp. 2969–2979, May 2023.

[9] Y. Li, K. Li, and S. Tong, "An observer-based fuzzy adaptive consensus control method for nonlinear multiagent systems," *IEEE Trans. Fuzzy Syst.*, vol. 30, no. 11, pp. 4667–4678, Nov. 2022.

[10] B. Ranjbar-Sahraei, F. Shabaninia, A. Nemati, and S.-D. Stan, "A novel robust decentralized adaptive fuzzy control for swarm formation of multiagent systems," *IEEE Trans. Ind. Electron.*, vol. 59, no. 8, pp. 3124–3134, Aug. 2012.

[11] Z.-G. Hou, L. Cheng, and M. Tan, "Decentralized robust adaptive control for the multiagent system consensus problem using neural networks," *IEEE Trans. Syst., Man, Cybern., B Cybern.*, vol. 39, no. 3, pp. 636–647, Jun. 2009.

[12] J. Ni and P. Shi, "Adaptive neural network fixed-time leader–follower consensus for multiagent systems with constraints and disturbances," *IEEE Trans. Cybern.*, vol. 51, no. 4, pp. 1835–1848, Apr. 2021.

[13] A.-M. Kang and H.-S. Yan, "Stability analysis and dynamic regulation of multi-dimensional Taylor network controller for SISO nonlinear systems with time-varying delay," *ISA Trans.*, vol. 73, pp. 31–39, Feb. 2018.

[14] Y.-Q. Han, "Adaptive tracking control of a class of nonlinear systems with unknown dead-zone output: A multi-dimensional Taylor network (MTN)-based approach," *Int. J. Control*, vol. 94, no. 11, pp. 3161–3170, Nov. 2021.

[15] G.-B. Wang, H.-S. Yan, and X.-Y. Zheng, "Contraction-based stochastic model predictive control for nonlinear systems with input delay using multidimensional Taylor network," *IEEE Trans. Autom. Control*, vol. 68, no. 12, pp. 7498–7513, Dec. 2023.

[16] M.-X. Wang, S.-L. Zhu, S.-M. Liu, Y. Du, and Y.-Q. Han, "Design of adaptive finite-time fault-tolerant controller for stochastic nonlinear systems with multiple faults," *IEEE Trans. Autom. Sci. Eng.*, vol. 20, no. 4, pp. 2492–2502, Oct. 2023.

[17] H. Min, S. Xu, and Z. Zhang, "Adaptive finite-time stabilization of stochastic nonlinear systems subject to full-state constraints and input saturation," *IEEE Trans. Autom. Control*, vol. 66, no. 3, pp. 1306–1313, Mar. 2021.

[18] H. Min, S. Xu, B. Zhang, and Q. Ma, "Output-feedback control for stochastic nonlinear systems subject to input saturation and time-varying delay," *IEEE Trans. Autom. Control*, vol. 64, no. 1, pp. 359–364, Jan. 2019.

[19] C. Wen, J. Zhou, Z. Liu, and H. Su, "Robust adaptive control of uncertain nonlinear systems in the presence of input saturation and external disturbance," *IEEE Trans. Autom. Control*, vol. 56, no. 7, pp. 1672–1678, Jul. 2011.

[20] S. L. Zhu and Y. Q. Han, "Adaptive decentralized prescribed performance control for a class of large-scale nonlinear systems subject to nonsymmetric input saturations," *Neural Comput. Appl.*, vol. 34, no. 13, pp. 11123–11140, Jul. 2022.

[21] S. Gao, H. Dong, B. Ning, and L. Chen, "Neural adaptive control for uncertain nonlinear system with input saturation: State transformation based output feedback," *Neurocomputing*, vol. 159, pp. 117–125, Jul. 2015.

[22] Z.-B. Song, P. Li, Z. Wang, X. Huang, and W.-H. Liu, "Adaptive tracking control for switched uncertain nonlinear systems with input saturation and unmodeled dynamics," *IEEE Trans. Circuits Syst. II, Exp. Briefs*, vol. 67, no. 12, pp. 3152–3156, Dec. 2020.

[23] Z. Liu et al., "A novel faster fixed-time adaptive control for robotic systems with input saturation," *IEEE Trans. Ind. Electron.*, vol. 71, no. 5, pp. 5215–5223, May 2024.

[24] M. Shahriari-Kahkeshi and M. Taj, "Distributed adaptive consensus tracking control for uncertain non-linear multi-agent systems with input saturation," *IET Control Theory Appl.*, vol. 13, no. 14, pp. 2153–2162, Sep. 2019.

[25] W.-J. Hao, J.-J. Sun, Z.-Y. Zong, S.-L. Zhu, and Y.-Q. Han, "Adaptive predefined time tracking control for nonlinear multi-agent systems subject to input saturation: An improved command filtering approach," *Nonlinear Dyn.*, vol. 110, pp. 1–20, Apr. 2025.

[26] X. Wang, H. Su, X. Wang, and G. Chen, "Fully distributed event-triggered semiglobal consensus of multi-agent systems with input saturation," *IEEE Trans. Ind. Electron.*, vol. 64, no. 6, pp. 5055–5064, Jun. 2017.

[27] X. Liu, J.-W. Xiao, D. Chen, and Y.-W. Wang, "Dynamic consensus of nonlinear time-delay multi-agent systems with input saturation: An impulsive control algorithm," *Nonlinear Dyn.*, vol. 97, no. 2, pp. 1699–1710, Jul. 2019.

[28] C. Liu, H. Wang, X. Liu, and Y. Zhou, "Adaptive finite-time fuzzy funnel control for nonaffine nonlinear systems," *IEEE Trans. Syst., Man, Cybern., Syst.*, vol. 51, no. 5, pp. 2894–2903, May 2021.

[29] S. Wang, X. Ren, J. Na, and T. Zeng, "Extended-state-observer-based funnel control for nonlinear servomechanisms with prescribed tracking performance," *IEEE Trans. Autom. Sci. Eng.*, vol. 14, no. 1, pp. 98–108, Jan. 2017.

[30] H. Wang, W. Bai, X. Zhao, and P. Liu, "Finite-Time-Prescribed performance-based adaptive fuzzy control for strict-feedback nonlinear systems with dynamic uncertainty and actuator faults," *IEEE Trans. Cybern.*, vol. 52, no. 7, pp. 6959–6971, Jul. 2022.

[31] Z.-B. Lin, Z. Liu, C.-Y. Su, Y.-N. Wang, C.-P. Chen, and Y. Zhang, "Adaptive fuzzy prescribed performance output-feedback cooperative control for uncertain nonlinear multiagent systems," *IEEE Trans. Fuzzy Syst.*, vol. 31, no. 12, pp. 4459–4470, Dec. 2023.

[32] C. P. Bechlioulis and G. A. Rovithakis, "Decentralized robust synchronization of unknown high order nonlinear multi-agent systems with prescribed transient and steady state performance," *IEEE Trans. Autom. Control*, vol. 62, no. 1, pp. 123–134, Jan. 2017.

[33] L.-T. Lu, S.-L. Zhu, D.-M. Wang, and Y.-Q. Han, "Distributed adaptive fault-tolerant control with prescribed performance for nonlinear multiagent systems," *Commun. Nonlinear Sci. Numer. Simul.*, vol. 138, Nov. 2024, Art. no. 108222.

[34] W.-J. He, S.-L. Zhu, L.-T. Lu, W. Zhao, and Y.-Q. Han, "Adaptive multi-switching-based global tracking control for switched nonlinear systems with prescribed performance," *IEEE Trans. Autom. Sci. Eng.*, vol. 21, no. 3, pp. 3243–3252, Jul. 2024.
[35] W. Wang, H. Liang, Y. Pan, and T. Li, "Prescribed performance adaptive fuzzy containment control for nonlinear multiagent systems using disturbance observer," *IEEE Trans. Cybern.*, vol. 50, no. 9, pp. 3879–3891, Sep. 2020.
[36] L. Yan, Z. Liu, C. L. P. Chen, Y. Zhang, and Z. Wu, "Optimized adaptive consensus control for multi-agent systems with prescribed performance," *Inf. Sci.*, vol. 613, pp. 649–666, Oct. 2022.
[37] K. Li, K. Zhao, and Y. Song, "Adaptive consensus of uncertain multi-agent systems with unified prescribed performance," *IEEE/CAA J. Autom. Sinica*, vol. 11, no. 5, pp. 1310–1312, May 2024.
[38] L. L. Zhang, W. W. Che, B. Chen, and C. Lin, "Adaptive fuzzy output-feedback consensus tracking control of nonlinear multiagent systems in prescribed performance," *IEEE Trans. Cybern.*, vol. 53, no. 3, pp. 1932–1943, Mar. 2023.
[39] K. Yong, M. Chen, Y. Shi, and Q. Wu, "Flexible performance-based robust control for a class of nonlinear systems with input saturation," *Automatica*, vol. 122, Dec. 2020, Art. no. 109268.
[40] H. Xie, G. Zong, D. Yang, X. Zhao, and Y. Yi, "Flexible-fixed-time-performance-based adaptive asymptotic tracking control of switched nonlinear systems with input saturation," *IEEE Trans. Autom. Sci. Eng.*, vol. 21, no. 4, pp. 6371–6382, Oct. 2024.
[41] M. Hashemi and G. Shahgholian, "Distributed robust adaptive control of high order nonlinear multi agent systems," *ISA Trans.*, vol. 74, pp. 14–27, Mar. 2018. [Online]. Available: https://www.sciencedirect.com/science/article/pii/S0019057816307881
[42] J. Huang, Y.-D. Song, W. Wang, C. Wen, and G. Li, "Smooth control design for adaptive leader-following consensus control of a class of high-order nonlinear systems with time-varying reference," *Automatica*, vol. 83, pp. 361–367, Sep. 2017. [Online]. Available: https://www.sciencedirect.com/science/article/pii/S0005109817303084
[43] A. Luo, Q. Zhou, H. Ma, and H. Y. Li, "Event-triggered optimal consensus control for MASs with multiple constraints: A flexible performance approach," *IEEE Trans. Autom. Sci. Eng.*, vol. 22, no. 3, pp. 13117–13127, Jun. 2025.
[44] H.-S. Yan and Z.-Y. Duan, "Tube-based model predictive control using multidimensional Taylor network for nonlinear time-delay systems," *IEEE Trans. Autom. Control*, vol. 66, no. 5, pp. 2099–2114, May 2021.
[45] Y.-Q. Han, "Adaptive tracking control for a class of stochastic non-linear systems with input delay: A novel approach based on multi-dimensional Taylor network," *IET Control Theory Appl.*, vol. 14, no. 15, pp. 2147–2153, Oct. 2020.
[46] D. Wang and J. Huang, "Neural network-based adaptive dynamic surface control for a class of uncertain nonlinear systems in strict-feedback form," *IEEE Trans. Neural Netw.*, vol. 16, no. 1, pp. 195–202, Jan. 2005.

**Wei-Jie Hao** received the B.S. degree in mathematics and applied mathematics from Qingdao University of Science and Technology, Qingdao, China, in 2023, where he is currently pursuing the M.S. degree.

His current research interests include adaptive control, neural networks, and nonlinear multi-agent systems.

**Zhao-Yi Zong** received the B.S. degree in mathematics and applied mathematics from Weifang University, Weifang, China, in 2024. She is currently pursuing the M.S. degree in Qingdao University of Science and Technology, Qingdao, China.

Her current research interests include adaptive control, neural networks, and nonlinear multi-agent systems.

**Shu-Zhen Wei** received the B.S. degree in mathematics and applied mathematics from Taishan University, Taian, China, in 2024. She is currently pursuing the M.S. degree with Qingdao University of Science and Technology.

Her current research interests include adaptive control, neural networks, nonlinear systems, and their applications.

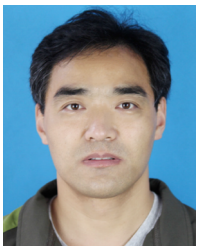

**Shan-Liang Zhu** received the M.S. degree from the School of Mathematical Sciences, Ocean University of China, in 2004 and the Ph.D. degree from the College of Electromechanical Engineering, Qingdao Science and Technology University, in 2020.

He is currently a Professor with Qingdao Science and Technology University. His research interests include differential dynamic systems, data driven control, machine learning, and their applications.

**Yu-Qun Han** received the B.S. degree in mathematics and applied mathematics and the M.S. degree in applied mathematics from Qingdao University of Science and Technology, Qingdao, China, in 2010 and 2013, respectively, and the Ph.D. degree in control theory and control engineering from Southeast University, Nanjing, in 2018. He has been with the School of Mathematics and Physics, Qingdao University of Science and Technology, Qingdao, China, since December 2018.

His current research interests include nonlinear system control, stochastic nonlinear system control, adaptive control, and neural networks.